Isotopic yields for the cold fission of ^{252}Cf

A. Sandulescu,[1–4] A. Florescu,[1,3,4] F. Carstoiu,[1] W. Greiner,[2–4] J. H. Hamilton,3 A. V. Ramayya,[3] and B. R. S. Babu[3]
[1]*Institute for Atomic Physics, Bucharest, P.O. Box MG-6, Romania*
[2]*Institut für Theoretische Physik der J.W. Goethe Universität, D-60054 Frankfurt am Main, Germany*
[3]*Physics Department, Vanderbilt University, Nashville, Tennessee 37235*
[4]*Joint Institute for Heavy Ion Research, Oak Ridge, Tennessee 37831*
(Received 15 December 1995)

The isotopic yields for the spontaneous cold fission of ^{252}Cf are predicted by using a double-folding potential and the M3Y nucleon-nucleon forces. The penetrabilities through this barrier are obtained within the one-dimensional WKB approximation. Realistic fragment ground-state deformations are used for the calculations. The results are in good agreement with zero neutron channel yields extracted from γ-γ-γ coincidence studies in the spontaneous fission of ^{252}Cf recorded with the early implementation Gammasphere. The double fine structure in such cold fragmentations has been experimentally observed for the first time. [S0556-2813(96)02707-0]

PACS number(s): 25.85.Ca, 24.75.+i, 27.90.+b

I. INTRODUCTION

In recent times, many new experimental data concerning the spontaneous cold fragmentations of nuclei have been obtained. These include exotic decays with emission of heavy clusters having masses from $A_L=12$ to 34 [1]. In addition the cold fission of many actinide nuclei produce fragments with masses from $\approx$ 70 to $\approx$ 166 atomic mass units [2–6]. Subsequently, several cases of such heavy clusters emitted with nearly zero internal excitation energy are now experimentally observed. They all confirm the theoretical predictions based on the idea of the cold rearrangements of large groups of nucleons from the ground state of the initial nucleus to the ground states of the two final fragments [7,8].

The existence of the so-called fusion valleys or ''cold'' valleys on the potential energy surfaces of the fission-prone heavy nuclei [7,9,10] proved to be a key ingredient for the prediction [7] and later for the interpretation of heavy cluster decays (the ^{208}Pb or ^{100}Sn valleys), or for the understanding of cold fission of the actinides (especially the ^{132}Sn valley). In all these situations the final fragments have compact shapes at the scission point and almost zero excitation energy. It has been shown that the transitions from the fission valley to the fusion valley along the fission path can qualitatively explain the cold fragmentation of the actinides [11]. Also the cluster decay model where the ground-state deformations of the final fragments are very important [12,13] is able to explain quantitatively the mass and charge yields in cold fission [14].

An extreme case is that of the bimodal fission observed for the Fm and Md isotopes [15] where the predominant fragmentations are close to two double magic ^{132}Sn nuclei. Here, two clearly distinct fission channels are observed, one with very high total kinetic energy (TKE) which practically exhausts the disintegration energy (Q value), corresponding to the fusion valley, and the second one at much lower TKE's which proceeds through the usual fission valley with elongated shapes.

For the cold fission studies, the Cf and Cm isotopes constitute a transition region between the lighter actinides such as Th, U, and Pu, and the bimodal fission region of Fm and Md nuclei. In the lighter actinides, the highest yields are observed when the heavier fragment is in the vicinity of ^{132}Sn and the lighter fragment is strongly deformed [6]. Indeed, the experimental data for ^{252}Cf (SF) [2] and ^{248}Cm (SF) [3] indicate a preference for cold fragmentations with both partners having pronounced ground-state deformations and masses $100\leqslant A_L\leqslant 114$, $140\leqslant A_H\leqslant 152$ respectively.

Very recently the first direct observation of cold (neutronless) fragmentation in the spontaneous fission of ^{252}Cf was made [4,5], using the multiple Ge-detector Compact Ball facility at Oak Ridge National Laboratory. Initially four pairs of neutronless fragmentations were observed: ^{104}Zr-^{148}Ce, ^{104}Mo-^{148}Ba, ^{106}Mo-^{146}Ba, and ^{108}Mo-^{144}Ba. More recently for a few pairs of fragments the ground band gamma cascades were accurately detected in both light and heavy partners with the early implementation Gammasphere using the triple-gamma coincidence technique [16].

It may be pointed out that the yields measured in the above-mentioned experiments are integrated yields. Up to now the yields in cold fission were measured as a function of TKE of the fragments, or as a function of their total excitation energy (TXE$=Q-$TKE). It was experimentally established that these yields increase strongly with the decrease of TKE's or equivalently with the increase of the final fragment TXE's. In the present experiments, based on triple-gamma coincidence of the lowest transitions in both fragments [16], most of the fragmentations are usually leading to higher excitations of the final nuclei which later on are decaying to the lowest states by gamma cascades. Evidently there are also splittings which leave the fragments in their ground or first excited states, but with lower probabilities. We are calling these experimentally determined yields as integrated yields due to the fact that they collect the contributions of all (neutronless) transitions over a whole range of fragment TXE's from zero up to at least the neutron binding energy, from where the evaporation of a first neutron becomes possible.

In cold fission, the two fragments are populated at low spins (0^+, 2^+, 4^+) and then decay by γ emission. While in the α decay the α particles are never excited (because of

their inert structure), in the cold fission process both fragments can be excited, hence the double fine structure. In the recent experiments [5,16] the double fine structure in the transitions leading to the final fragments was observed directly for the first time in the cold fission decays, similar to the well-known fine structure revealed in the alpha decays and even in heavier cluster decays of odd-mass nuclei. In alpha decay of even-even and odd-A heavy nuclei the transitions are observed not only to the ground state of the final nuclei, but also to some of their low excited states [17]. These could be states belonging to the rotational ground-state band or rotational beta or gamma bands in even-even nuclei, or states belonging to some rotational bands built on intrinsic quasiparticle states in odd-A final nuclei. It was noted early [18–20] that the alpha transitions in odd-A nuclei exhibited reduced widths ranging from values similar to those of neighboring even-even nuclei down to much smaller values. When the transition proceeds to a final state with no change in the single-particle configuration of the last odd nucleon, a ''favored'' transition is observed, with an alpha reduced width comparable to those in neighboring even-even nuclei. Other ''unfavored'' transitions will be nevertheless observed in some cases in the same nucleus, if they lead to the ground state or other low states of the daughter nucleus and their decay energy is high enough. Consequently many alpha-emitting nuclei exhibit a fine structure in their alpha transitions. In the past few years fine structure was also discovered for some heavy cluster-emitting nuclei, e.g., for the ^{14}C transitions in ^{223}Ra [21]. In a similar way, the cold (neutronless) fission of heavy nuclei could leave both final fragments on some low excited states and a double fine structure of the transitions is observed for those cases.

In this paper we present an estimation of the isotopic yields for different fragmentations of the nucleus ^{252}Cf in spontaneous cold fission using only the barrier penetrabilities. For the evaluation of the potential barrier between the final fragments we used the M3Y nucleon-nucleon forces. We found that the yields are very sensitive to the fragment's quadrupole deformation. In the present estimations no octupole or higher deformations were taken into account.

II. THE POTENTIAL BARRIER FROM M3Y FORCES

In the present paper we evaluated the nuclear plus Coulomb interaction between two coaxial deformed fragments with the help of the double-folding M3Y potential defined [23] as

$$V_{M3Y}(R)=\int d\mathbf{r}_1 d\mathbf{r}_2 \rho_1(\mathbf{r}_1)\rho_2(\mathbf{r}_2)v(\mathbf{r}_{12}), \tag{1}$$

which contains the corresponding nucleon-nucleon interaction [24]

$$v(\mathbf{r}_{12})=v_{00}(r_{12})+\hat{J}_{00}\delta(\mathbf{r}_{12})+v_{01}(r_{12})\tau_1\cdot\tau_2+\frac{e^2}{r_{12}}, \tag{2}$$

where

$$\mathbf{r}_{12}=\mathbf{R}+\mathbf{r}_2-\mathbf{r}_1 .$$

The central component of the M3Y force in Eq. (2) is

$$v_{00}(r)=\left[7999\frac{e^{-4r}}{4r}-2134\frac{e^{-2.5r}}{2.5r}\right]\ \text{MeV}$$

and the isospin part has the form

$$v_{01}(r)=\left[-4885.5\frac{e^{-4r}}{4r}+1175.5\frac{e^{-2.5r}}{2.5r}\right]\ \text{MeV}.$$

The second term in Eq. (2) approximates the single-nucleon exchange effects through a zero-range pseudopotential ($\hat{J}_{00}=-262$ MeV fm^3). The spin-spin v_{10} and spin-isospin v_{11} components are disregarded since their final contributions tend to be very small.

The two final nuclei are viewed as coaxial spheroids (''nose-to-nose'' configuration) with nuclear density

$$\rho(\mathbf{r})=\rho_0\left[1+\exp\frac{1}{a}\left(r-\frac{R_0}{c}(1+\beta_2 Y_2^0(\cos\theta))\right)\right]^{-1} \tag{3}$$

with the constant ρ_0 fixed by normalizing the proton and neutron density to the Z proton and N neutron numbers, respectively, the diffusivity $a=0.5$ fm and $R_0=r_0A^{1/3}$ with $r_0=1.12$ fm. Here β_2 is the quadrupole deformation and c is the usual constant which ensures the volume conservation condition

$$\int_V d^3r=\frac{4\pi}{3}R_0^3$$

from which it follows

$$c(\beta_2)=\left[1+\frac{3}{4\pi}\beta_2^2+\frac{1}{14\pi}\sqrt{\frac{5}{4\pi}}\beta_2^3\right]^{1/3}.$$

We computed the double-folded deformed potential barrier by making a general multipole expansion of the potential [25,26], which for two final nuclei with orientation in space given through the Euler angles Ω_1 and Ω_2 can be written

$$V(\mathbf{R},\Omega_1,\Omega_2)=\sum_{\lambda_i,\mu_i} V^{\mu_1\mu_2\mu_3}_{\lambda_1\lambda_2\lambda_3}(R)D^{\lambda_1}_{\mu_1 0}(\Omega_1)D^{\lambda_2}_{\mu_2 0}(\Omega_2)Y^{\mu_3}_{\lambda_3}(\hat{R}). \tag{4}$$

In our case, with both final fragments aligned along the same symmetry axis [$\hat{R}=(0,0)$, $\Omega_1=\Omega_2=(0,0,0)$] we obtain

$$V(R)=\sum_{\lambda_i} V^{0\,0\,0}_{\lambda_1\lambda_2\lambda_3}(R) \tag{5}$$

with

$$V^{0\,0\,0}_{\lambda_1\lambda_2\lambda_3}=\frac{2}{\pi}(C^{\lambda_1\lambda_2\lambda_3}_{0\,0\,0})^2\times\int r_1^2 dr_1 r_2^2 dr_2 \rho_{\lambda_1}(r_1)\rho_{\lambda_2}(r_2)F_{\lambda_1\lambda_2\lambda_3}(r_1,r_2,R), \tag{6}$$

where $C^{\lambda_1\lambda_2\lambda_3}_{0\,0\,0}$ is a Clebsch-Gordan coefficient, $F_{\lambda_1\lambda_2\lambda_3}$ is the double-folding kernel [25] which is easy to evaluate for

Yukawa and Coulomb-type interactions, and ρ_λ are the multipole components of the corresponding expansion of the nuclear densities

$$\rho(\mathbf{r}) = \sum_{\lambda \text{even}} \rho_\lambda(r) Y_\lambda^0(\hat{r}) \tag{7}$$

which in turn have the form of Eq. (3).

III. RESULTS OF THE CALCULATIONS

The latest experimental developments utilizing multidetector facilities and multiple-gamma coincidences permitted the outburst of many fine structure data for the cold fission, similar to those known for a long time in alpha decay, and more recently in heavy cluster decays. For the cold (neutronless) fragmentation of a heavy nucleus, we considered that the two final nuclei are in their ground states or in the first one or two excited states, usually belonging to the ground-state rotational band or other rotational bands built on intrinsic quasiparticle states. For these transitions, we calculated the penetrability through the double-folded potential barrier by using the corresponding Q values. Due to the inherent ambiguities of different final channels (e.g., fragment deformations, channel radii, and so on) we assumed that the cluster preformation probabilities are similar for all possible splittings and consequently we used the same frequency factor ν for the collisions with the fission barrier for all fragmentations. Henceforth in our calculations we are neglecting the preformation factors for different channels. Our relative isotopic yields computed below correspond to those cold (neutronless) fragmentations with both final nuclei emitted in their ground state. Consequently the theoretical isotopic yields are not integrated over a domain of TXE values, like the experimental yields mentioned above, but are resulting for zero total excitation energy.

We estimated the penetrability through the double-folded potential barrier in the framework of the WKB approximation

$$P = \exp\left(-\frac{2}{\hbar} \int_{R_i}^{R_o} \sqrt{2\mu[V(R) - Q]}\, dR \right), \tag{8}$$

where R is the distance between the fragment mass centers, R_i and R_o are the inner and outer turning points defined by

$$V(R_i) = V(R_o) = Q \tag{9}$$

and $\mu = A_H A_L / (A_H + A_L)$ is the reduced mass of the binary system, since the most important part of the potential barrier is extended outside the touching point between the two fragments.

The accurate evaluation of the Q values is very important since the WKB penetrabilities are very sensitive to them. We obtained the Q values from recent experimental mass tables [27], and for some of the fragmentations the masses were taken from the extended tables of Ref. [28] generated within a macroscopic-microscopic model.

The deformation parameters which we used were also taken from the tables of Ref. [28], and for some isotopes we employed the deformation values deduced from cold fission data [12,14] which are similar or slightly larger in some cases (e.g., 5%–8% larger for the Sr, Zr, and Mo isotopes) than those from [28]. The calculated values of the penetrabilities are very sensitive to the assumed deformations of the final fragments, since a 10% increase in the β_2 values leads up to an order of magnitude increase of the penetrabilities. Consequently our calculated penetrabilities should contain an uncertainty factor of about 10. Nevertheless, the relative yields should not change significantly. Of course, the higher multipoles like the octupole can play an important role bringing about additional uncertainties.

The calculated penetrabilities $P(A_L, Z_L)$ are given in Table I, together with the isotopic yields $Y(A_L, Z_L)$,

$$Y(A_L, Z_L) = \frac{P(A_L, Z_L)}{\Sigma_{A_L Z_L} P(A_L, Z_L)}, \tag{10}$$

for the most frequent spontaneous cold neutronless fragmentations of ^{252}Cf. As we see, the highest yields are obtained for fragment masses $98 \leqslant A_L \leqslant 110$ and $142 \leqslant A_H \leqslant 154$, and for fragment charges $38 \leqslant Z_L \leqslant 44$ and $54 \leqslant Z_H \leqslant 60$, respectively.

Experimentally the half-life of ^{252}Cf is 2.54 yr and the branching ratios for its alpha decay and spontaneous fission are 97% and 3%, respectively [29]. Taking an energy of zero-point ground-state vibrations of about 1 MeV, we obtain a collision frequency ν with the fission barrier of 2.5×10^{20} s^{-1} and a penetrability through this barrier

$$P_0 = \frac{\ln 2}{\nu t_{1/2}(\text{s.f.})} \approx 0.11 \times 10^{-29}. \tag{11}$$

Since we already calculated the WKB penetrabilities $P(A_L, Z_L)$ through the cold fission barrier, Eq. (8), we are able to predict also the partial half-lives for the cluster decays corresponding to the cold neutronless fragmentations as

$$t_{1/2}(A_L, Z_L) = \frac{\ln 2}{\nu P_0 P(A_L, Z_L)}. \tag{12}$$

These calculated partial half-lives are also given in Table I. Low partial half-lives are resulting for splittings such as ^{106,107}Nb+^{146,145}La and $^{107-110}$Mo+$^{145-142}$Ba where an enhanced production is experimentally observed at very low total excitation energy of the fission fragments [2].

The theoretical penetrabilities and isotopic yields predicted by the present cluster model depend on the Q values for the cold fragmentations, and also on the ground-state deformations of the final nuclei. In fact, from the 29 mass splits shown in Table I, in 13 cases the highest yield is attained by those charge splits which have lower Q values but higher deformation of one or both fragments.

The recent experiment of cold fragmentation in the spontaneous fission of ^{252}Cf [4,5,16] permitted the direct observation of neutronless fission channels for the light fragments $^{96-100}$Sr, $^{100-104}$Zr, $^{104-108}$Mo , $^{110-112}$Ru, and ^{116}Pd in coincidence with the corresponding heavy fragments, for which the isotopic yields were determined. The neutronless fission channels within a few MeV TXE range involve gamma cascades following the transition to some definite energy levels in the two final fragments. We should like to mention that some contributions to these channels involve gamma-ray

TABLE I. The results of the calculation for the first three most probable charge fragmentations Z_L/Z_H for every mass fragmentation A_L/A_H. Here ϵ_2 are the fragment quadrupole deformations ($\epsilon_2 \approx 0.95\beta_2$). The penetrabilities P were obtained from Eq. (8), the relative isotopic yields Y from Eq. (10), and the partial half-lives $t_{1/2}$ from Eq. (12).

A_L/A_H	Z_L/Z_H	ϵ_{2L}	ϵ_{2H}	Q (MeV)	P	Y (%)	$t_{1/2}$ (s)
94/158	36/62	0.270	0.300	202.52	2.70×10^{-8}	0.52	9.33×10^{16}
	38/60	0.215	0.295	209.06	2.14×10^{-8}	0.41	1.18×10^{17}
	37/61	0.227	0.290	203.53	6.33×10^{-11}	1×10^{-3}	3.98×10^{19}
95/157	38/60	0.249	0.300	207.25	9.87×10^{-9}	0.19	2.55×10^{17}
	37/61	0.255	0.275	204.11	5.59×10^{-10}	1×10^{-2}	4.51×10^{18}
	36/62	0.310	0.300	198.94	3.97×10^{-10}	8×10^{-3}	6.34×10^{18}
96/156	38/60	0.240	0.290	209.12	1.15×10^{-7}	2.22	2.19×10^{16}
	39/59	0.287	0.320	206.48	2.11×10^{-9}	4×10^{-2}	1.20×10^{18}
	37/61	0.320	0.280	201.48	3.21×10^{-10}	6×10^{-3}	7.86×10^{18}
97/155	38/60	0.277	0.280	206.83	9.83×10^{-9}	0.19	2.56×10^{17}
	39/59	0.272	0.320	207.63	8.70×10^{-9}	0.17	2.90×10^{17}
	37/61	0.320	0.270	201.43	1.93×10^{-10}	4×10^{-3}	1.31×10^{19}
98/154	38/60	0.330	0.230	208.25	2.10×10^{-7}	4.04	1.20×10^{16}
	39/59	0.307	0.320	206.17	5.30×10^{-9}	0.10	4.76×10^{17}
	40/58	0.255	0.283	209.92	7.32×10^{-10}	1×10^{-2}	3.44×10^{18}
99/153	38/60	0.350	0.270	205.27	4.43×10^{-8}	0.85	5.69×10^{16}
	39/59	0.291	0.290	207.77	7.65×10^{-9}	0.15	3.30×10^{17}
	40/58	0.279	0.288	208.80	7.14×10^{-10}	1×10^{-2}	3.53×10^{18}
100/152	38/60	0.350	0.250	206.41	1.26×10^{-7}	2.43	2.00×10^{16}
	40/58	0.273	0.267	211.69	3.22×10^{-8}	0.62	7.84×10^{16}
	39/59	0.320	0.282	206.79	5.88×10^{-9}	0.11	4.29×10^{17}
101/151	40/58	0.325	0.240	210.95	4.78×10^{-8}	0.92	5.27×10^{16}
	39/59	0.325	0.255	207.73	1.04×10^{-8}	0.20	2.42×10^{17}
	41/57	0.314	0.270	209.61	5.24×10^{-10}	1×10^{-2}	4.81×10^{18}
102/150	40/58	0.340	0.200	212.76	3.76×10^{-7}	7.24	6.70×10^{15}
	39/59	0.340	0.280	205.92	4.51×10^{-9}	9×10^{-2}	5.59×10^{17}
	41/57	0.309	0.266	209.54	3.18×10^{-10}	6×10^{-3}	7.93×10^{18}
103/149	40/58	0.330	0.236	211.20	1.35×10^{-7}	2.60	1.86×10^{16}
	41/57	0.322	0.231	212.64	3.27×10^{-8}	0.63	7.70×10^{16}
	39/59	0.350	0.260	205.61	1.72×10^{-9}	3×10^{-2}	1.47×10^{18}
104/148	42/56	0.315	0.245	214.41	1.05×10^{-7}	2.02	2.40×10^{16}
	40/58	0.300	0.210	212.80	7.00×10^{-8}	1.35	3.60×10^{16}
	41/57	0.340	0.254	211.42	5.59×10^{-8}	1.08	4.51×10^{16}
105/147	42/56	0.330	0.230	214.86	3.29×10^{-7}	6.34	7.66×10^{15}
	41/57	0.310	0.230	214.13	3.02×10^{-7}	5.82	8.34×10^{15}
	40/58	0.340	0.200	210.57	1.12×10^{-8}	0.22	2.25×10^{17}
106/146	41/57	0.340	0.252	212.17	3.13×10^{-7}	6.03	8.05×10^{15}
	42/56	0.245	0.200	217.33	1.42×10^{-8}	0.27	3.40×10^{16}
	40/58	0.330	0.170	211.91	1.25×10^{-8}	0.24	2.02×10^{17}
107/145	42/56	0.290	0.210	217.02	3.75×10^{-7}	7.22	6.72×10^{15}
	41/57	0.300	0.240	214.05	3.54×10^{-7}	6.82	7.12×10^{15}
	43/55	0.333	0.200	215.29	1.42×10^{-8}	0.27	1.78×10^{17}
108/144	42/56	0.245	0.198	218.61	1.68×10^{-7}	3.24	1.50×10^{16}
	43/55	0.320	0.215	215.29	2.01×10^{-8}	0.39	1.25×10^{17}
	44/54	0.300	0.200	216.94	5.46×10^{-9}	0.11	4.62×10^{17}
109/143	43/55	0.290	0.200	218.28	2.69×10^{-7}	5.18	9.36×10^{15}
	42/56	0.300	0.177	217.34	2.38×10^{-7}	4.58	1.06×10^{16}
	44/54	0.300	0.185	217.28	3.85×10^{-9}	7×10^{-2}	6.55×10^{17}
110/142	43/55	0.300	0.190	217.91	1.50×10^{-7}	2.89	1.68×10^{16}
	42/56	0.250	0.150	219.53	7.14×10^{-8}	1.38	3.53×10^{16}
	44/54	0.240	0.150	221.65	1.89×10^{-8}	0.36	1.33×10^{17}

TABLE I. (*Continued*).

A_L/A_H	Z_L/Z_H	ϵ_{2L}	ϵ_{2H}	Q (MeV)	P	Y (%)	$t_{1/2}$ (s)
111/141	43/55	0.270	0.150	220.32	1.25×10^{-7}	2.41	2.02×10^{16}
	45/53	0.320	0.190	218.80	9.98×10^{-8}	1.92	2.53×10^{16}
	44/54	0.260	0.150	221.14	3.91×10^{-8}	0.75	6.45×10^{16}
112/140	44/54	0.220	0.120	224.65	1.96×10^{-7}	3.78	1.29×10^{16}
	45/53	0.280	0.190	220.41	1.45×10^{-7}	2.79	1.74×10^{16}
	43/55	0.300	0.140	219.00	6.06×10^{-8}	1.17	4.16×10^{16}
113/139	45/53	0.270	0.110	223.66	1.17×10^{-7}	2.25	2.15×10^{16}
	44/54	0.220	0.120	223.83	4.33×10^{-8}	0.83	5.82×10^{16}
	43/55	0.260	0.110	220.71	1.14×10^{-8}	0.22	2.21×10^{17}
114/138	45/53	0.240	0.080	225.32	4.09×10^{-8}	0.79	6.16×10^{16}
	44/54	0.180	0.060	227.04	1.31×10^{-8}	0.25	1.92×10^{17}
	46/52	0.150	0.140	225.45	1.08×10^{-9}	2×10^{-2}	2.33×10^{18}
115/137	45/53	0.200	0.070	226.93	1.88×10^{-8}	0.36	1.34×10^{17}
	46/52	0.160	0.110	225.99	7.92×10^{-10}	2×10^{-2}	3.18×10^{18}
	44/54	0.180	0.030	225.19	4.88×10^{-11}	1×10^{-3}	5.16×10^{19}
116/136	46/52	0.140	0.060	230.40	1.77×10^{-8}	0.34	1.42×10^{17}
	45/53	0.200	0.050	227.48	1.38×10^{-8}	0.27	1.83×10^{17}
	44/54	0.150	-0.020	227.61	7.66×10^{-12}	1×10^{-4}	3.29×10^{20}
117/135	46/52	0.160	0.045	230.39	2.62×10^{-8}	0.51	9.62×10^{16}
	45/53	0.160	0.040	229.36	9.54×10^{-9}	0.18	2.64×10^{17}
	47/51	0.180	0.020	227.98	1.01×10^{-10}	2×10^{-3}	2.48×10^{19}
118/134	46/52	0.100	0.000	233.96	3.61×10^{-9}	7×10^{-2}	6.98×10^{17}
	45/53	0.230	-0.010	225.72	8.15×10^{-11}	2×10^{-3}	3.09×10^{19}
	47/51	0.160	-0.030	229.65	7.02×10^{-12}	1×10^{-4}	3.59×10^{20}
119/133	47/51	0.160	-0.040	233.54	4.27×10^{-9}	8×10^{-2}	5.90×10^{17}
	46/52	0.160	-0.030	231.01	2.55×10^{-10}	5×10^{-3}	9.89×10^{18}
	45/53	0.220	-0.030	225.85	1.12×10^{-11}	2×10^{-4}	2.26×10^{20}
120/132	47/51	0.150	-0.020	231.72	3.54×10^{-10}	7×10^{-3}	7.12×10^{18}
	48/50	0.030	-0.010	236.62	7.66×10^{-11}	2×10^{-3}	3.29×10^{19}
	46/52	0.110	-0.050	232.01	3.23×10^{-12}	6×10^{-5}	7.80×10^{20}
121/131	47/51	0.140	-0.050	232.60	7.52×10^{-11}	1×10^{-3}	3.35×10^{19}
	48/50	0.050	-0.030	234.36	1.22×10^{-12}	2×10^{-5}	2.07×10^{21}
	46/52	0.110	0.000	228.14	1.91×10^{-13}	4×10^{-6}	1.32×10^{22}
122/130	47/51	0.150	-0.030	229.85	5.84×10^{-12}	1×10^{-4}	4.31×10^{20}
	46/52	0.080	0.000	227.66	4.71×10^{-15}	9×10^{-8}	5.35×10^{23}
	49/49	0.080	-0.030	229.60	2.23×10^{-15}	4×10^{-8}	1.13×10^{24}

side feeding from other rotational bands built upon vibrational states or quasiparticle states of the fragments. Therefore these integrated (at least up to the neutron binding energy) isotopic yields for neutronless splittings are some orders of magnitude higher than the isotopic yields determined as a function of the fragment TXE or fragment kinetic energies, see, e.g., [2], for spontaneous fission of ^{252}Cf and [6] for thermal neutron-induced fission of ^{233}U. Moreover, the calculated yields do not include differences in the level densities near the ground states of the even-even and odd-odd nuclei. Including the differences in level densities will enhance all odd-odd yields relative to the even-even ones.

IV. THE EXPERIMENTAL DATA

In order to search for events corresponding to zero neutron channels the γ-γ-γ coincidences events produced in the spontaneous fission of ^{252}Cf were recorded with early implementation Gammasphere. A γ-γ-γ ''cube'' was built using the RADWARE program. The ''cube'' data were analyzed by setting two gates, one on the $2^+\rightarrow0^+$ transition and the other on the $4^+\rightarrow2^+$ transition in a particular even-even nucleus and the corresponding γ rays of its correlated partner nuclei were analyzed. The peak areas of the γ rays were then corrected for efficiency and internal conversion. In the majority of the cases only the $2^+\rightarrow0^+$ transition intensity of the partner was used to extract the zero neutron channel yield. After the efficiency correction, the resulting areas for all the neutron channels were summed and the areas for the individual channels were divided by the resulting sum to get the relative fraction of the events for each neutron channel. Furthermore to obtain the zero neutron channel yields per 100 fission events, our above yields were then normalized to the integrated yield for the partner computed by Wahl [30]. The results including $2n$, $4n$, $6n$, etc., channels are fitted with a Gaussian to check for internal consistency. Table II

TABLE II. The experimental isotopic yields Y_{expt} per 100 fission events.

A_L/Z_L	A_H/Z_H	Y_{expt}
96/38	156/60	0.02 ± 0.01
98/38	154/60	0.08 ± 0.02
100/38	152/60	0.05 ± 0.02
100/40	152/58	0.12 ± 0.04
102/40	150/58	0.02 ± 0.01
104/40	148/58	0.02 ± 0.01
104/42	148/56	0.02 ± 0.01
106/42	146/56	0.08 ± 0.05
108/42	144/56	0.15 ± 0.06 [a]
110/44	142/54	0.10 ± 0.05
112/44	140/54	0.04 ± 0.02
116/46	136/52	0.05 ± 0.02
99/38	153/60	0.30 ± 0.10
103/40	149/58	0.10 ± 0.01
105/42	147/56	0.20 ± 0.07
107/42	145/56	0.24 ± 0.06
111/44	141/54	0.14 ± 0.06 [b]

[a]The ^{108,104}Mo peaks are very difficult to strip in this case.
[b]The 150 keV transition in ^{111}Ru was used to obtain this result.

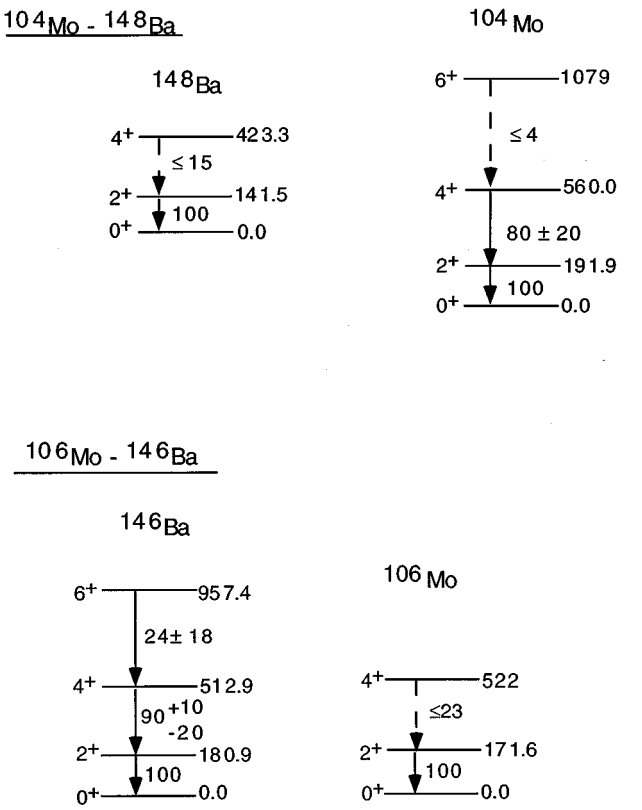

FIG. 1. Relative level populations of the lowest excited states of fission fragments of ^{252}Cf obtained in two zero-neutron even-even Mo/Ba splittings. The transition $2^+\rightarrow0^+$ is normalized to 100.

gives the zero neutron yields obtained from the recent ^{252}Cf data [16]. The yields for ^{108}Mo-^{144}Ba and ^{110}Ru-^{142}Xe have large uncertainties because of the very nearly identical energies of the 2^+ states in ^{108}Mo, ^{104}Mo and ^{110}Ru, ^{108}Ru nuclei, respectively. We should like to mention that only the pairs for which the spectra are known could be considered. In a few cases, we also present in Table II our results for odd-odd fragmentations which are a factor of 3–5 larger than the yields for the even-even cases. For odd-Z fragmentations, the spectra are too complicated to extract useful information from the present data. Higher yields for the odd-odd fragmentations of ^{252}Cf are also observed by Hambsch *et al.* [2] for low TXE values (TXE$\leqslant$9 MeV). One can see from Table II that the zero neutron yields are of the order of 5×10^{-2} per 100 Cf fission events.

The values of the theoretical relative yields (Table I) and experimental yields (Table II) should not be compared directly since the latter values are integrated yields (over the internal excitation energies of the final fragments, at least up to the binding energy of the last neutron) while the former ones are yields corresponding only to transitions to the ground states of the final fragments. Nevertheless the trends for both quantities should be very similar, i.e., larger theoretical yields will indicate that also larger experimental yields could be observed for the same cold (neutronless) fragmentation.

Using the triple-gamma coincidence technique the double fine structure in the neutronless fission of ^{252}Cf could be detected. In Fig. 1 are shown the level populations, relative to the $2^+\rightarrow0^+$ transition which is normalized to 100, for the fission fragments from ^{252}Cf obtained for two even-even Mo-Ba pairs, including the relative transition probabilities to the first 2^+,4^+, and 6^+ excited states of the rotational band built upon the 0^+ ground state. For comparison in Fig. 2 are shown the complete ground-state rotational bands for the same fragments, observed for all fission channels. It is evident that in the cold (neutronless) even-even splittings only the lowest levels of the ground-state rotational bands are populated. This fact supports the dynamical beta-stretching model for cold fission [14] which assumes only a coaxial motion of the fragments at the scission configuration. Since other vibrational states corresponding to the kinking and bending modes between fragments at the scission point were not observed in the present experiment, it is possible that other 0^+ beta-phonon states populated in the fission fragments could be observed in the future. In the odd and odd-odd fragments, with higher isotopic yields, the beta-phonon states are coupled to the one- or many-quasiparticle states leading to a more complicated energy level landscape and to higher level densities. Such transitions can be easily detected by using two back-to-back ionization chambers for measuring the TKE in coincidence with the gamma-ray cascades in both fragments.

Recently cold fission isotopic yields for ^{233}U(n_{th},f) were extrapolated to TXE=0 MeV by Schwab *et al.* [6]. Their calculated yields per level are higher for the ground-state even-even fragmentations, since the level density for this case is the lowest. These even-even splittings should correspond to the well-known favored alpha and heavier cluster transitions in even-even nuclei. Nevertheless we expect that, in analogy with the other cluster decays and by not taking into account the influence of the Q values on the cluster penetrabilities, many hindrance factors close to unity could

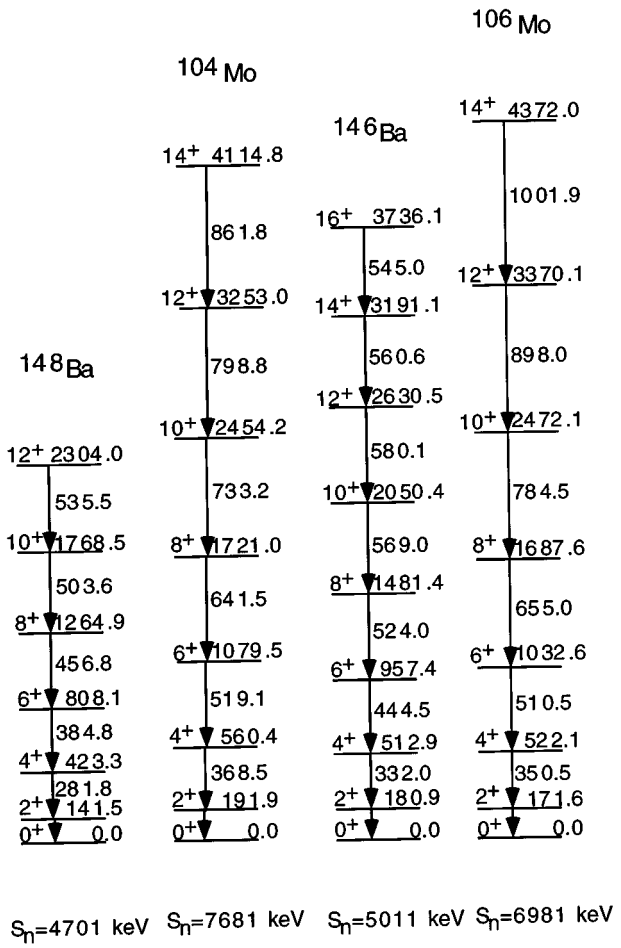

FIG. 2. The ground-state bands observed for the ^{104}Mo-^{148}Ba and ^{106}Mo-^{146}Ba pairs as separated fragments.

be observed in odd or odd-odd cold fission fragmentations which lead to low energy levels in both final nuclei. The cold fission isotopic yields calculated recently [22] for the same ^{234}U compound nucleus using a level density formalism based on the backshifted Fermi gas model [31] and the dynamical beta-stretching model [14] agreed well with the experimental data [6]. Thus the ambiguities due to the estimation of level densities close to the ground state of even-even fragments [6] were avoided and it was confirmed that the odd splittings of cold fragmentations have higher isotopic yields than the even-even ones. This will allow a new spectroscopy with heavy clusters by determining the corresponding cluster preformation factors. Consequently, we are able to predict that favored transitions should be observable in all types of cold fragmentations.

V. DISCUSSION AND CONCLUSIONS

We have shown here that a simple cluster model is able to predict correctly the most important cold fragmentations observed in the spontaneous cold fission of the nucleus ^{252}Cf . The double-folding potential barrier with M3Y nucleon-nucleon forces gives relative isotopic yields $Y(A_L, Z_L)$ with higher values for cluster masses $98 \leqslant A_L \leqslant 110$ and $142 \leqslant A_H \leqslant 154$ and, respectively, cluster charges $38 \leqslant Z_L \leqslant 44$ and $54 \leqslant Z_H \leqslant 60$. In these regions both the light and the heavy fragments have important ground-state deformations that give rise to potential barriers between the two final nuclei which are significantly lowered, leading to increased penetrabilities and yields. Nevertheless the scission configurations for these cold fragmentations are still much more compact than in the case of usual ''hot'' fission.

We should mention here that a striking feature of the cold fission yields close to the highest TKE values permitted by the Q values [2,3,5] is the fact that many odd-odd splittings have values larger than the neighboring even-even fragmentations. This feature of cold fragmentations suggests that either the cold fission yields are influenced by the level density of the fragments [6,22] or that the deformations of odd fragments are larger than for the corresponding even ones. Indeed, the calculated potential barriers are depending on the deformation of the final fragments. For increased deformations of the two coaxial nuclei, their touching point distance (the distance between their centers of mass when the fragment tips are in contact) increases also. In this case the barrier height is lowered and within our model we obtain increased penetrabilities and higher yields.

In order to determine more exactly the double fine structure in cold fission one of the new large detector arrays like Gammasphere has to be used. In the future the theory can be further centered on studying new cases of neutronless cold fragmentations, especially the odd-odd ones which should have yields larger than the even-even splittings. Thus further experimental and theoretical studies of the double fine structure in cold fission decays can open up new insights into cold fragmentation phenomena.

[1] P.B. Price, Nucl. Phys. **A502**, 41c (1989).
[2] F.-J. Hambsch, H.-H. Knitter, and C. Budtz-Jorgensen, Nucl. Phys. **A554**, 209 (1993).
[3] A. Benoufella, G. Barreau, M. Asghar, P. Audouard, F. Brisard, T.P. Doan, M. Hussonnois, B. Leroux, J. Trochon, and M.S. Moore, Nucl. Phys. **A565**, 563 (1993).
[4] J.H. Hamilton, A.V. Ramayya, J. Kormicki, W.C. Ma, Q. Lu, D. Shi, J.K. Deng, S.J. Zhu, A. Sandulescu, W. Greiner, G.M. Ter-Akopian, Yu.Ts. Oganessian, G.S. Popeko, A.V. Daniel, J. Kliman, V. Polhorsky, M. Morhac, J.D. Cole, R. Aryaeinejad, I.Y. Lee, N.R. Johnson, and F.K. McGowan, J. Phys. G **20**, L85 (1994).
[5] G.M. Ter-Akopian, J.H. Hamilton, Yu.Ts. Oganessian, J. Kormicki, G.S. Popeko, A.V. Daniel, A.V. Ramayya, Q. Lu, K. Butler-Moore, W.-C. Ma, J.K. Deng, D. Shi, J. Kliman, V. Polhorsky, M. Morhac, W. Greiner, A. Sandulescu, J.D. Cole, R. Aryaeinejad, N.R. Johnson, I.Y. Lee, and F.K. McGowan, Phys. Rev. Lett. **73**, 1477 (1994).
[6] W. Schwab, H.-G. Clerc, M. Mutterer, J.P. Theobald, and H. Faust, Nucl. Phys. **A577**, 674 (1994).
[7] A. Sandulescu and W. Greiner, J. Phys. G **3**, L189 (1977).
[8] A. Sandulescu and W. Greiner, Rep. Prog. Phys. **55**, 1423 (1992).

[9] P. Moller, J.R. Nix, and W.J. Swiatecki, Nucl. Phys. **A469**, 1 (1987).
[10] S. Cwiok, P. Rozmej, A. Sobiczewski, and Z. Patyk, Nucl. Phys. **A491**, 281 (1989).
[11] J.F. Berger, M. Girod, and D. Gogny, Nucl. Phys. **A428**, 23c (1984).
[12] A. Sandulescu, A. Florescu, and W. Greiner, J. Phys. G **15**, 1815 (1989).
[13] F. Gönnenwein and B. Borsig, Nucl. Phys. **A530**, 27 (1991).
[14] A. Florescu, A. Sandulescu, C. Cioaca, and W. Greiner, J. Phys. G **19**, 669 (1993).
[15] E.R. Hulet, J.F. Wild, R.J. Dougan, R.W. Lougheed, J.H. Landrum, A.D. Dougan, M. Schadel, R.L. Hahn, P.A. Baisden, C.M. Henderson, R.J. Dypzyk, K. Summerer, and G.R. Bethune, Phys. Rev. Lett. **56**, 313 (1986).
[16] A.V. Ramayya, J.H. Hamilton, B.R.S. Babu, S.J. Zhu, L.K. Peker, T.N. Ginter, J. Kormicki, W.C. Ma, J.D. Cole, R. Aryaeinejad, K. Butler-Moore, Y.X. Dardenne, M.W. Drigert, G.M. Ter-Akopian, Yu.Ts. Oganessian, J.O. Rasmussen, S. Asztalos, I.Y. Lee, A.O. Macchiavelli, S.Y. Chu, K.E. Gregorich, M.F. Mohar, S. Prussin, M.A. Stoyer, R.W. Lougheed, K.J. Moody, J.F. Wild, A. Sandulescu, A. Florescu, and W. Greiner, in Proceedings of the International Conference on Nuclear Structure: ''Structure of Vacuum and Elementary Matter,'' 1996, Wilderness, South Africa (World Scientific, in press).
[17] L. Rosenblum, C. R. Acad. Sci. Paris **188**, 1401 (1929).
[18] A. Bohr, P.O. Fröman, and B.R. Mottelson, Dan. Mat. Fys. Medd. **29**, 10 (1955).
[19] A. Sandulescu, Nucl. Phys. **37**, 332 (1962).
[20] J.O. Rasmussen, in *Alpha, Beta, and Gamma-Ray Spectroscopy*, edited by K. Siegbahn (North-Holland, Amsterdam, 1965), Vol. 1, p. 701.
[21] E. Hourani, L. Rosier, G. Berrier-Ronsin, A. Elayi, A.C. Mueller, G. Rappenecker, G. Rotbard, G. Renou, A. Liebe, L. Stab, and H.L. Ravn, Phys. Rev. C **44**, 1424 (1991).
[22] V. Avrigeanu, A. Florescu, A. Sandulescu, and W. Greiner, Phys. Rev. C **52**, R1755 (1995).
[23] G.R. Satchler and W.G. Love, Phys. Rep. **55**, 183 (1979).
[24] G. Bertsch, J. Borysowicz, H. McManus, and W.G. Love, Nucl. Phys. **A284**, 399 (1977).
[25] F. Carstoiu and R.J. Lombard, Ann. Phys. (N.Y.) **217**, 279 (1992).
[26] A. Sandulescu, R.K. Gupta, W. Greiner, F. Carstoiu, and M. Horoi, Int. J. Mod. Phys. E **1**, 379 (1992).
[27] A.H. Wapstra, G. Audi, and R. Hoeckstra, At. Data Nucl. Data Tables **39**, 281 (1988).
[28] P. Möller, J.R. Nix, W.D. Myers, and W.J. Swiatecki, At. Data Nucl. Data Tables **59**, 185 (1995).
[29] A. Rytz, At. Data Nucl. Data Tables **47**, 205 (1991).
[30] A.C. Wahl, At. Data Nucl. Data Tables **39**, 1 (1988).
[31] M. Grossjean and H. Feldmeier, Nucl. Phys. **A444**, 115 (1985).